LETTERS
PUBLISHED ONLINE: 15 DECEMBER 2014 | DOI: 10.1038/NMAT4148
nature materials

Negative capacitance in a ferroelectric capacitor

Asif Islam Khan[1], Korok Chatterjee[1], Brian Wang[1], Steven Drapcho[2], Long You[1], Claudy Serrao[1], Saidur Rahman Bakaul[1], Ramamoorthy Ramesh[2,3,4] and Sayeef Salahuddin[1,4]*

The Boltzmann distribution of electrons poses a fundamental barrier to lowering energy dissipation in conventional electronics, often termed as Boltzmann Tyranny[1-5]. Negative capacitance in ferroelectric materials, which stems from the stored energy of a phase transition, could provide a solution, but a direct measurement of negative capacitance has so far been elusive[1-3]. Here, we report the observation of negative capacitance in a thin, epitaxial ferroelectric film. When a voltage pulse is applied, the voltage across the ferroelectric capacitor is found to be decreasing with time—in exactly the opposite direction to which voltage for a regular capacitor should change. Analysis of this 'inductance'-like behaviour from a capacitor presents an unprecedented insight into the intrinsic energy profile of the ferroelectric material and could pave the way for completely new applications.

Owing to the energy barrier that forms during the phase transition and separates the two degenerate polarization states, a ferroelectric material could show negative differential capacitance while in non-equilibrium[1–5]. The state of negative capacitance is unstable, but just as a series resistance can stabilize the negative differential resistance of an Esaki diode, it is also possible to stabilize a ferroelectric in the negative differential capacitance state by using a series dielectric capacitor[1–3]. In this configuration, the ferroelectric acts as a 'transformer' that boosts the input voltage. The resulting amplification could lower the voltage needed to operate a transistor below the limit otherwise imposed by the Boltzmann distribution of electrons[1–5]. For this reason, the possibility of a transistor that exploits negative differential capacitance has been widely studied in recent years[6–15]. However, despite the fact that negative differential capacitance has been predicted by the standard Landau model going back to the early days of ferroelectricity[16–20], a direct measurement of this effect has never been reported. In this work, we demonstrate a negative differential capacitance in a thin, single-crystalline ferroelectric film, by constructing a simple R–C network and monitoring the voltage dynamics across the ferroelectric capacitor.

We start by noting that capacitance is, by definition, a small signal concept—capacitance C at a given charge Q_F is related to the potential energy U by the relation $C=[d^2U/dQ_F^2]^{-1}$. For this reason we shall henceforth use the term 'negative capacitance' to refer to 'negative differential capacitance'. For a ferroelectric material, as shown in Fig. 1a, the capacitance is negative only in the barrier region around $Q_F=0$. Starting from an initial state P, as a voltage is applied across the ferroelectric capacitor, the energy landscape is tilted and the polarization will move to the nearest local minimum. Figure 1b shows this transition for a voltage that is smaller than the coercive voltage V_c. If the voltage is larger than V_c, one of the minima disappears and Q_F moves to the remaining minimum of the energy landscape (Fig. 1c). Notably, as the polarization state descends in Fig. 1c, it passes through the region where $C=[d^2U/dQ_F^2]^{-1}<0$. Therefore, while switching from one stable polarization to the other, a ferroelectric material passes through a region where the differential capacitance is negative.

To experimentally demonstrate the above, we applied voltage pulses across a series combination of a ferroelectric capacitor and a resistor R and observed the time dynamics of the ferroelectric polarization. A 60 nm film of ferroelectric $Pb(Zr_{0.2}Ti_{0.8})O_3$ (PZT) was grown on metallic $SrRuO_3$ (60 nm)-buffered $SrTiO_3$ substrate using the pulsed laser deposition technique. Square gold top electrodes with a surface area $A=(30\,\mu m)^2$ were patterned on top of the PZT films using standard micro-fabrication techniques. The remnant polarization of the PZT film is measured to be $\sim 0.74\,C\,m^{-2}$ and the coercive voltages are roughly $+2.1$ V and -0.8 V. A resistance value $R=50\,k\Omega$ is used as the series resistor. Figure 2a shows the schematic diagram of the experimental set-up and Fig. 2b shows the equivalent circuit diagram. The capacitor C connected in parallel with the ferroelectric capacitor in Fig. 2b represents the parasitic capacitance contributed by the probe station and the oscilloscope in the experimental set-up, which was measured to be ~ 60 pF. An a.c. voltage pulse sequence of V_S: $-5.4\,V \rightarrow +5.4\,V \rightarrow -5.4\,V$ was applied as input. The total charge in the ferroelectric and parasitic capacitors at a given time t, $Q(t)$, is calculated using $Q(t)=\int_0^t i_R(t)dt$, with i_R being the current flowing through R. The charge across the ferroelectric capacitor $Q_F(t)$ is calculated using the relation: $Q_F(t)=Q(t)-CV_F(t)$, with V_F being the voltage measured across the ferroelectric capacitor. Figure 2c shows the transients corresponding to V_S, V_F, i_R and Q. We note in Fig. 2c that after the $-5.4\,V \rightarrow +5.4\,V$ transition of V_S, V_F increases until point A, after which it decreases until point B. We also note in Fig. 2c that, during the same time segment AB, i_R is positive and Q increases. In other words, during the time segment AB, the changes in V_F and Q have opposite signs. As such, dQ/dV_F is negative during AB, indicating that the ferroelectric polarization is passing through the unstable states. A similar signature of negative capacitance is observed after the $+5.4\,V \rightarrow -5.4\,V$ transition of V_S during the time segment CD in Fig. 2c. The charge density of the ferroelectric capacitor or the ferroelectric polarization, $P(t)=Q_F(t)/A$, is plotted as a function of $V_F(t)$ in Fig. 3a, from which we can observe in that the $P(t)$–$V_F(t)$ curve is hysteretic, and for sections AB and CD the slope of the curve is negative, indicating that the capacitance is negative in these regions.

We also experimented with a.c. voltage pulses of different amplitudes and two different values of the series resistance. The $P(t)$–$V_F(t)$ characteristic is found to be qualitatively similar (see Supplementary Section 2 for detailed measurements). There are, however, some interesting differences. For example, Fig. 3b shows

[1]Department of Electrical Engineering and Computer Sciences, University of California, Berkeley, California 94720, USA. [2]Department of Physics, University of California, Berkeley, California 94270, USA. [3]Department of Material Science and Engineering, University of California, Berkeley, California 94270, USA. [4]Material Science Division, Lawrence Berkeley National Laboratory, Berkeley, California 94270, USA. *e-mail: sayeef@berkeley.edu

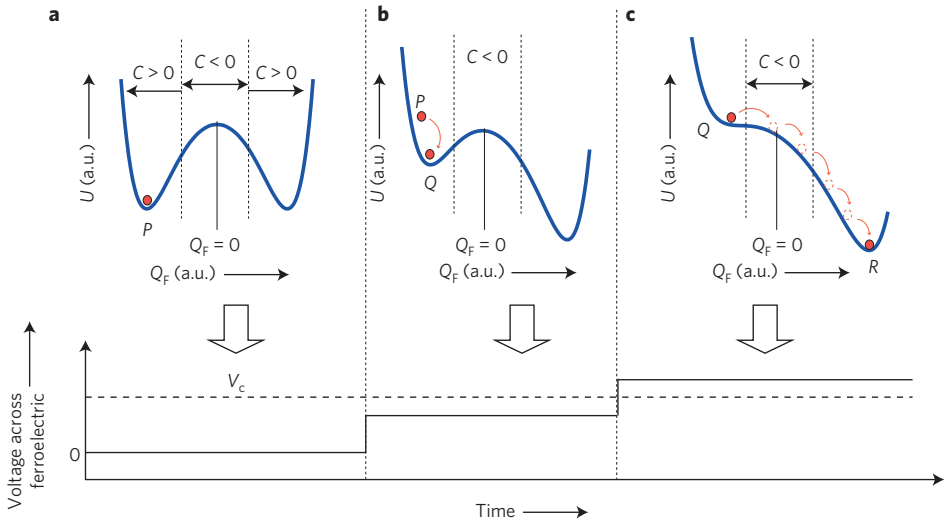

Figure 1 | Energy landscape description of the ferroelectric negative capacitance. a, Energy landscape U of a ferroelectric capacitor in the absence of an applied voltage. The capacitance C is negative only in the barrier region around charge $Q_F = 0$. **b**,**c**, Evolution of the energy landscape on the application of a voltage across the ferroelectric capacitor that is smaller (**b**) or greater (**c**) than the coercive voltage V_c. If the voltage is greater than the coercive voltage, the ferroelectric polarization descends through the negative capacitance states. *P, Q* and *R* represent different polarization states in the energy landscape.

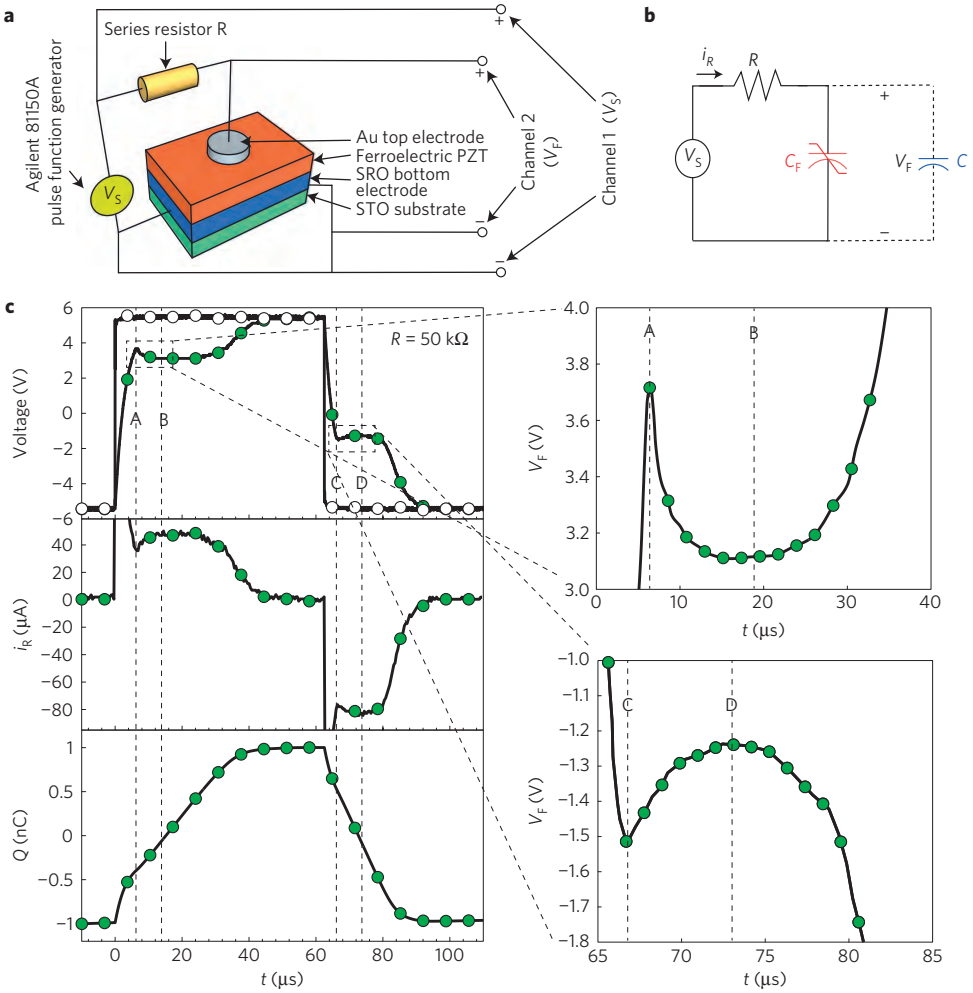

Figure 2 | Transient response of a ferroelectric capacitor. a, Schematic diagram of the experimental set-up. **b**, Equivalent circuit diagram of the experimental set-up. C_F, C and R represent the ferroelectric and the parasitic capacitor and the external resistor, respectively. V_S, V_F and i_R are the source voltage, the voltage across C_F and the current through R, respectively. **c**, Transients corresponding to the source voltage V_S, the ferroelectric voltage V_F and the charge Q on the application of an a.c. voltage pulse V_S: −5.4 V → +5.4 V → −5.4 V. R = 50 kΩ. Negative capacitance transients are observed during the time segments AB and CD. The source voltage pulse is shown as the line connecting open circles and transients as the lines connecting green circles.

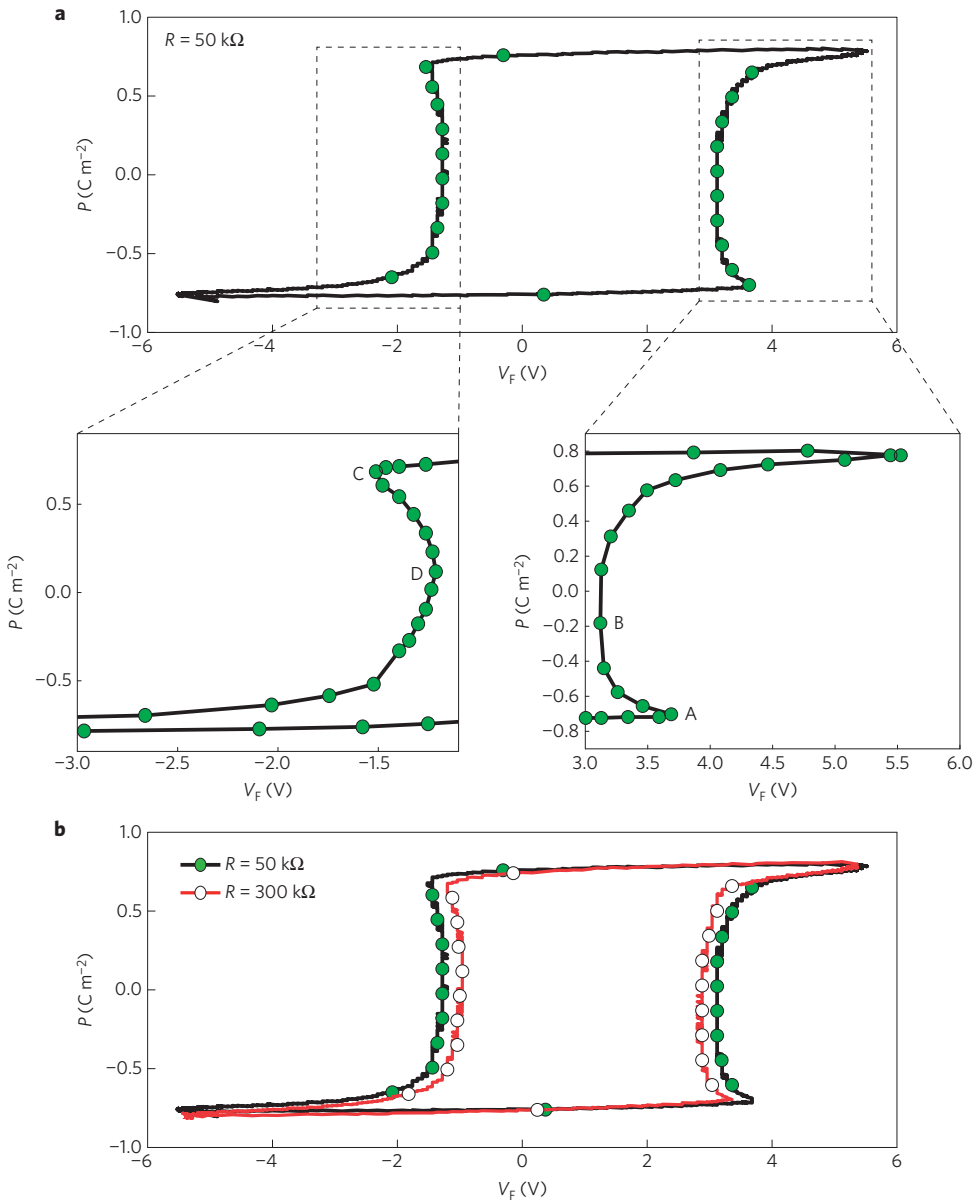

Figure 3 | Experimental measurement of negative capacitance. a, Ferroelectric polarization $P(t)$ as a function of $V_F(t)$ with $R = 50\,k\Omega$ for V_S: $-5.4\,V \rightarrow +5.4\,V \rightarrow -5.4\,V$. In sections AB and CD, the slope of the $P(t) - V_F(t)$ curve is negative, indicating a negative capacitance in these regions. **b**, Comparison of the $P(t) - V_F(t)$ curves corresponding to $R = 50\,k\Omega$ and $300\,k\Omega$ for V_S: $-5.4\,V \rightarrow +5.4\,V \rightarrow -5.4\,V$.

a comparison of the $P(t)$–$V_F(t)$ curves corresponding to $R = 50\,k\Omega$ and $300\,k\Omega$ for V_S: $-5.4\,V \rightarrow +5.4\,V \rightarrow -5.4\,V$. We note that for a smaller value of R the hysteresis loop is wider, which we discuss later.

We simulated the experimental circuit shown in Fig. 2b, starting from the Landau–Khalatnikov equation[16],

$$\rho \frac{dQ_F}{dt} = -\frac{dU}{dQ_F} \quad (1)$$

where the energy density $U = \alpha Q_F^2 + \beta Q_F^4 + \gamma Q_F^6 - Q_F V_F$. α, β and γ are the anisotropy constants and ρ is a material dependent parameter that accounts for dissipative processes during the ferroelectric switching. Equation (1) leads to an expression for the voltage across the ferroelectric capacitor:

$$V_F = \frac{Q_F}{C_F(Q_F)} + \rho \frac{dQ_F}{dt} \quad (2)$$

where $C_F(Q_F) = (2\alpha Q_F + 4\beta Q_F^3 + 6\gamma Q_F^5)^{-1}$. From equation (2), we note that the equivalent circuit for a ferroelectric capacitor consists of an internal resistor ρ and a nonlinear capacitor $C_F(Q_F)$ connected in series. We shall denote $Q_F/C_F(Q_F)$ as the internal ferroelectric node voltage V_{int}. Figure 4a shows the corresponding equivalent circuit. The transients in the circuit were simulated by solving equation (2). Figure 4b shows the transients corresponding to V_S, V_F, V_{int}, i_R and Q on the application of a voltage pulse V_S: $-14\,V \rightarrow +14\,V \rightarrow -14\,V$ with $R = 50\,k\Omega$ and $\rho = 50\,k\Omega$. In Fig. 4b, we observe opposite signs of changes in V_F and Q during the time segments AB and CD, as was seen experimentally in Fig. 2b. We also note that the P–V_F curve shown in Fig. 4c is hysteretic, as was observed experimentally in Fig. 2d. To understand the difference between the P–V_F and P–V_{int} curves we note that $V_F = V_{int} + i_F\rho$, with i_F being the current through the ferroelectric branch; the additional resistive voltage drop, $i_F\rho$, results in the hysteresis in the P–V_F curve. Nevertheless, it is clear from Fig. 4c that the negative slope of the P–V_{int} curve in a certain range of P, due to C_F being

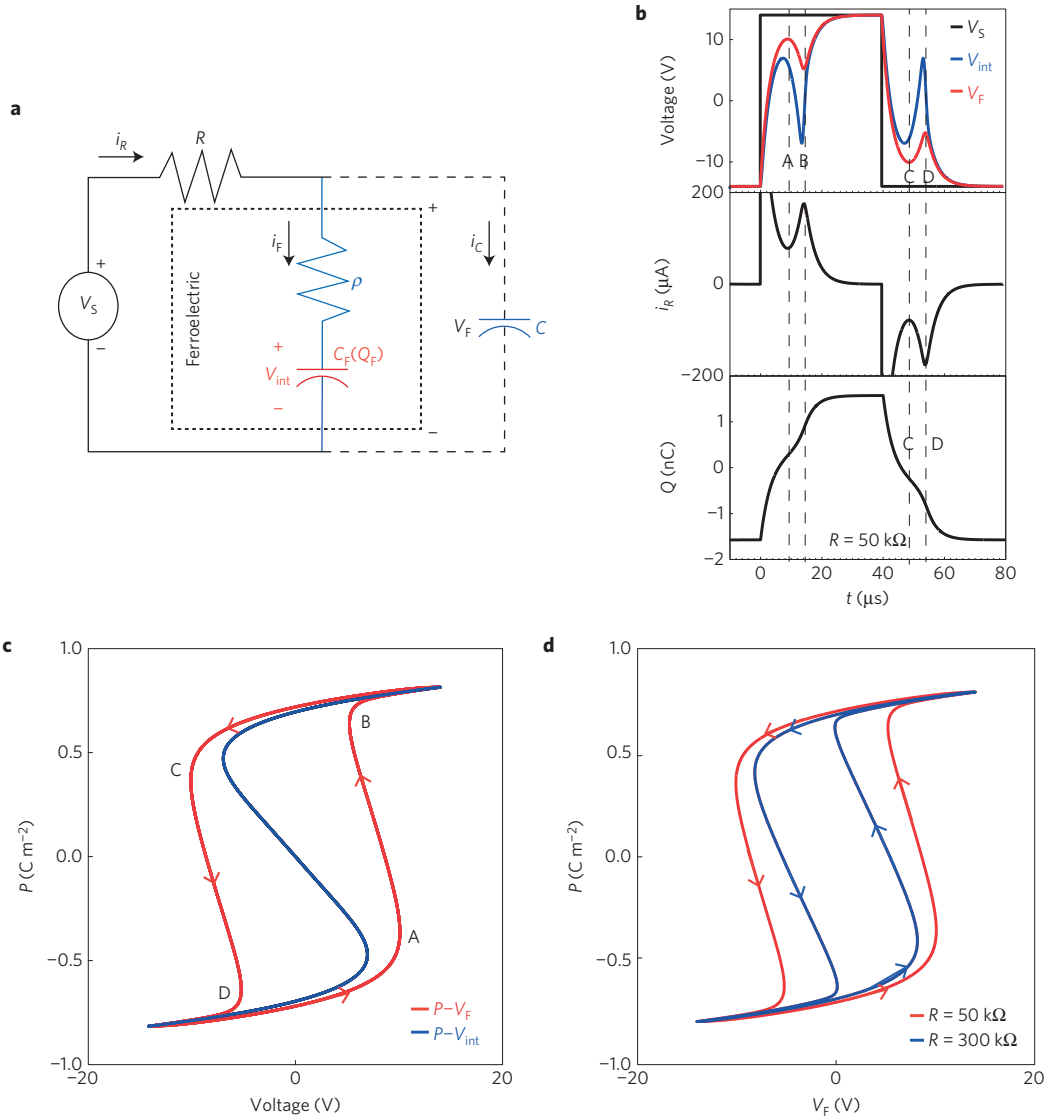

Figure 4 | Simulation of the time dynamics of the ferroelectric switching. a, Equivalent circuit diagram of the simulation. C_F, ρ, C and R represent the ferroelectric capacitor, the internal resistor, the parasitic capacitor and the external resistor, respectively. V_S, V_{int} and V_F are the voltages across the source and the capacitors C_F and C, respectively. i_R, i_F and i_C are the currents through R, C_F and C, respectively. **b**, Simulated transients corresponding to the source voltage V_S, the ferroelectric voltage V_F and the charge Q on the application of a voltage pulse V_S: $-14\,V \rightarrow +14\,V \rightarrow -14\,V$. **c**, Ferroelectric polarization $P(t)$ as a function of $V_F(t)$ and $V_{int}(t)$. **d**, Comparison of the simulated $P(t)$-$V_F(t)$ curves for $R = 50\,k\Omega$ and $200\,k\Omega$ on the application of V_S: $-14\,V \rightarrow +14\,V \rightarrow -14\,V$.

negative in that range, is reflected by the negative slope in the P–V_F curve in the segments AB and CD.

We also simulated the transients for the same circuit with $R = 200\,k\Omega$ for V_S: $-14\,V \rightarrow +14\,V \rightarrow -14\,V$. Figure 4d compares the simulated P–V_F curves for $R = 50\,k\Omega$ and $200\,k\Omega$. We observe that, for a smaller value of R, the hysteresis loop of the simulated P–V_F curve is wider, as was observed experimentally in Fig. 3b. This is due to the fact that, for a larger R, the current through the ferroelectric is smaller, resulting in a smaller voltage drop across ρ. The value of the internal resistance ρ can be extracted by comparing experimentally measured P–V_F curves for two different values of R for the same voltage pulse: $\rho(P) = (V_{F1}(P) - V_{F2}(P))/(i_{F1}(P) - i_{F2}(P))$. Here $V_F(P)$ and $i_F(P)$ are the voltage across and the current through the ferroelectric material, respectively. Indices 1 and 2 denote values for two different values of R. The average value of ρ is found to decrease monotonically from a value of $\sim 15\,k\Omega$ with an increasing amplitude of the applied voltage, whereas the average magnitude of the negative capacitance remains reasonably constant within the range 400–500 pF (Supplementary Fig. 17). Interestingly, this value of the negative capacitance is similar to that extracted by stabilizing PZT in a negative capacitance state by an in-series STO capacitor[9] (Supplementary Section 8).

If the applied voltage amplitude is smaller than the coercive voltage, such that the ferroelectric lies in one of the potential wells (Fig. 1a), its capacitance is positive and so it should behave just like a simple capacitor. On the other hand, if the applied voltage amplitude is larger than the coercive voltage, the ferroelectric switches and a negative capacitance transient is expected. This is exactly what is observed in our experiments (Supplementary Section 4.3). The fact that in the same circuit both positive and negative capacitance transients can be achieved just by changing the amplitude of the voltage also indicates that any influence of the parasitic components, if present, is minimal. Also, detailed measurements (Supplementary Section 3) show that the influence of defects is also minimal. Furthermore, the observed effect is robust against material variations. Supplementary Section 9 shows

data for a different material stack, where the PZT thickness is increased to 100 nm and the bottom electrode is changed from SRO to $La_{0.7}Sr_{0.3}MnO_3$ (20 nm). A similar negative capacitance transient is observed.

The addition of a series resistance (R) is critically important in revealing the negative capacitance region in the dynamics. An appreciable voltage drop across the series resistance R allows the voltage across the ferroelectric capacitor to be measured without being completely dominated by the source voltage—in the limit when $R \rightarrow 0$, the voltmeter would be directly connected across the voltage source. Indeed, most model studies[18,21–23] have been done in the latter limit where the ferroelectric capacitor is directly connected across a voltage source (or through a small resistance). Note that the dynamics in our experiments is intentionally slowed down by adding a large series resistance. The duration of the negative capacitance transient can be probed by varying the value of the series resistance and is found to be less than 20 ns for the given PZT thickness and electrode size (Supplementary Section 7).

A negative slope in the polarization–voltage characteristic has been predicted since the early days of ferroelectricity[16–20]. An S-like polarization–voltage behaviour in one branch of the hysteresis has been measured in a transistor structure[13]. However, a successful measurement of the entire intrinsic hysteresis loop has been performed only indirectly[20]. In contrast, our results provide a direct measure of the intrinsic hysteresis and negative capacitance of the material. Given the size of the capacitor used (30 μm × 30 μm), the switching invariably occurs through domain-mediated mechanisms. Importantly, our results show that, even in such a domain-mediated switching, a regime of abrupt switching is present that leads to negative capacitance transience. Thus, the double-well picture shown in Fig. 1a, which is typically associated with a single-domain configuration (equation (1)), can still qualitatively predict the experimental outcome. Interestingly, from Fig. 2c, it is clear that the negative capacitance ensues in the initial period of the switching. This indicates that microscopically abrupt switching events dominate the early part of the dynamics. By varying the external stimuli, it is also possible to probe the behaviour of intrinsic parameters such as ρ (Supplementary Section 6) that govern the ferroelectric switching.

Before concluding, it is worth noting that the concept of negative capacitance goes beyond the ferroelectric hysteresis and can be applied in general to a two-state system separated by an intrinsic barrier (stored energy)[24–28]. The measurement presented here could provide a generic way to probe the intrinsic negative capacitance in all such systems. A robust measurement of the negative capacitance could provide a guideline for stabilization, which could then overcome Boltzmann Tyranny in field-effect transistors, as mentioned earlier. The inductance-like behaviour observed in this experiment could also lead to many other applications, such as negating capacitances in an antenna, boosting voltages at various part of a circuit, developing coil-free resonators and oscillators, and so on.

Received 15 April 2014; accepted 24 October 2014; published online 15 December 2014

References

1. Salahuddin, S. & Datta, S. Use of negative capacitance to provide voltage amplification for low power nanoscale devices. *Nano Lett.* **8,** 405–410 (2008).
2. Zhirnov, V. V. & Cavin, R. K. Negative capacitance to the rescue. *Nature Nanotech.* **3,** 77–78 (2008).
3. Theis, T. N. & Solomon, P. M. It's time to reinvent the transistor. *Science* **327,** 1600–1601 (2010).
4. Theis, T. N. & Solomon, P. M. In quest of the next switch: Prospects for greatly reduced power dissipation in a successor to the silicon field-effect transistor. *Proc. IEEE* **98,** 2005–2014 (2010).
5. Ionescu, A. M. & Riel, H. Tunnel field-effect transistors as energy-efficient electronic switches. *Nature* **479,** 329–337 (2011).
6. Dubourdieu, C. *et al.* Switching of ferroelectric polarization in epitaxial $BaTiO_3$ films on silicon without a conducting bottom electrode. *Nature Nanotech.* **8,** 748–754 (2013).
7. Salahuddin, S. & Datta, S. *Proc. Intl. Electron Devices Meeting* (*IEDM*) (IEEE, 2008).
8. Rusu, A., Salvatore, G. A., Jiménez, D. & Ionescu, A. M. *Proc. Intl. Electron Devices Meeting* (*IEDM*) (IEEE, 2010).
9. Khan, A. I. *et al.* Experimental evidence of ferroelectric negative capacitance in nanoscale heterostructures. *Appl. Phys. Lett.* **99,** 113501 (2011).
10. Appleby, D. J. *et al.* Experimental observation of negative capacitance in ferroelectrics at room temperature. *Nano Lett.* **14,** 3864–3868 (2014).
11. Gao, W. *et al.* Room-temperature negative capacitance in a ferroelectric–dielectric superlattice heterostructure. *Nano Lett.* **14,** 5814–5819 (2014).
12. Khan, A. I., Yeung, C., Hu, C. & Salahuddin, S. *Proc. Intl. Electron Devices Meeting* (*IEDM*) (IEEE, 2011).
13. Salvatore, G. A., Rusu, A. & Ionescu, A. M. Experimental confirmation of temperature dependent negative capacitance in ferroelectric field effect transistor. *Appl. Phys. Lett.* **100,** 163504 (2012).
14. Then, H. W. *et al. Proc. Intl. Electron Devices Meeting* (*IEDM*) (IEEE, 2013).
15. The International Technology Roadmap for Semiconductors, Emerging Research Devices (2011); www.itrs.net/Links/2011itrs/home2011.htm
16. Landau, L. D. & Khalatnikov, I. M. On the anomalous absorption of sound near a second order phase transition point. *Dokl. Akad. Nauk* **96,** 469–472 (1954).
17. Lines, M. E. & Glass, A. M. *Principles and Applications of Ferroelectrics and Related Materials* (Clarendon, 2001).
18. Merz, W. J. Switching time in ferroelectric $BaTiO_3$ and its dependence on crystal thickness. *J. Appl. Phys.* **27,** 938–943 (1956).
19. Bratkovsky, A. M. & Levanyuk, A. P. Very large dielectric response of thin ferroelectric films with the dead layers. *Phys. Rev. B* **63,** 132103 (2001).
20. Bratkovsky, A. M. & Levanyuk, A. P. Depolarizing field and "real" hysteresis loops in nanometer-scale ferroelectric films. *Appl. Phys. Lett.* **89,** 253108 (2006).
21. Larsen, P. K. *et al.* Nanosecond switching of thin ferroelectric films. *Appl. Phys. Lett.* **59,** 611–613 (1991).
22. Li, J. *et al.* Ultrafast polarization switching in thin-film ferroelectrics. *Appl. Phys. Lett.* **84,** 1174–1176 (2004).
23. Jiang, A. Q. *et al.* Subpicosecond domain switching in discrete regions of $Pb(Zr_{0.35}Ti_{0.65})O_3$ thick films. *Adv. Funct. Mater.* **22,** 2148–2153 (2012).
24. Jana, R. K., Snider, G. L. & Jena, D. On the possibility of sub 60 mV/decade subthreshold switching in piezoelectric gate barrier transistors. *Phys. Status Solidi C* **10,** 1469–1472 (2013).
25. AbdelGhany, M. & Szkopek, T. Extreme sub-threshold swing in tunnelling relays. *Appl. Phys. Lett.* **104,** 013509 (2014).
26. Masuduzzaman, M. & Alam, M. A. Effective nanometer airgap of NEMS devices using negative capacitance of ferroelectric materials. *Nano Lett.* **14,** 3160–3165 (2014).
27. Eisenstein, J. P., Pfeiffer, L. N. & West, K. W. Negative compressibility of interacting two-dimensional electron and quasiparticle gases. *Phys. Rev. Lett.* **68,** 674–677 (1992).
28. Li, L. *et al.* Very large capacitance enhancement in a two-dimensional electron system. *Science* **332,** 825–828 (2011).

Acknowledgements

This work was supported in part by the Office of Naval Research (ONR), the Center for Low Energy Systems Technology (LEAST), one of the six SRC STARnet Centers, sponsored by MARCO and DARPA and the NSF E3S Center at Berkeley. A.I.K. acknowledges the Qualcomm Innovation Fellowship 2012–2013.

Author contributions

A.I.K. and C.S. grew the PZT films. A.I.K., K.C., B.W. and S.D. performed the time-dependence measurements. A.I.K., L.Y., C.S. and S.R.B. performed the structural and electrical characterization of the thin films. A.I.K. and S.S. conceived and designed the experiment. All authors discussed the results and commented on the manuscript.

Additional information

Supplementary information is available in the online version of the paper. Reprints and permissions information is available online at www.nature.com/reprints. Correspondence and requests for materials should be addressed to S.S.

Competing financial interests

The authors declare no competing financial interests.